Journal Name

ARTICLE TYPE

Cite this: DOI: 10.1039/xxxxxxxxxx

SUPPORTING INFORMATION: Solvent-shared pairs of densely charged ions induce intense but short-range supra-additive slowdown of water rotation†

Ana Vila Verde,* Mark Santer, Reinhard Lipowsky

Received Date
Accepted Date

DOI: 10.1039/xxxxxxxxxx

www.rsc.org/journalname

1 Parameterizing anion-cation interactions

The anion-cation interactions are optimized against the experimentally determined solution activity derivative at 2.5 m. This property directly depends on ion-ion interactions, thus making it an excellent target for parameterization. We opt for this indirect approach because directly parameterizing anion-cation interactions from quantum mechanical calculations is not feasible, as described below. The activity derivative can be easily calculated in simulations using the Kirkwood-Buff (KB) solution theory[1,2], as summarized below. Approaches based on the KB theory have been successfully used to optimize anion-cation interaction parameters involving non-polarizable models of simple monovalent and divalent ions[3–7] or between water and neutral solutes[7–9], lending confidence to this choice.

1.1 Kirkwood-Buff theory

The Kirkwood-Buff theory of solutions is described in detail elsewhere[1–5,7,8,10,11] so here only a brief summary is presented. KB theory relates integrals of the radial distribution functions in the grand canonical ensemble (μVT) to macroscopic thermodynamic properties. The KB integrals are defined as

$$G_{ij} = 4\pi \int_0^\infty r^2 \left[g_{ij}^{\mu VT}(r) - 1 \right] dr \tag{1}$$

In this expression, $g_{ij}^{\mu VT}(r)$ is the radial distribution function of species j around species i in the μVT ensemble. To obey the condition of electroneutrality, cations and anions cannot be treated separately when applying this theory to electrolyte solutions. Instead, anions and cations are assumed indistinguishable and the electrolyte solution is treated as a binary system composed of water (w) and co-solvent (c). The number density, ρ_c, of the co-solvent is then $\rho_c = n_c/V = (n_+ + n_-)/V$, where n_+ is the number of cations, n_- is the number of anions, and V is the volume of the system. The molar activity derivative, a_{cc}, of an electrolyte solution is defined as

$$a_{cc} = \left. \frac{\partial \ln a_c}{\partial \ln \rho_c} \right|_{P,T} \tag{2}$$

where a_c is the solution molar activity and is experimentally accessible. The molar activity derivative can be expressed in terms of the integrals

$$G_{cc} = \frac{1}{4}(2G_{+-} + G_{++} + G_{--}) \tag{3}$$

and

$$G_{cw} = G_{w+} + G_{w-} \tag{4}$$

as

$$a_{cc} = \frac{1}{1 + \rho_c(G_{cc} - G_{cw})} \tag{5}$$

In these expressions, the subscripts $(c, w, +, -)$ indicate the pairs of particles for which the KB integrals are calculated.

1.1.1 Calculating Kirkwood-Buff integrals from simulations of closed systems

Simulating open systems of dense fluids is challenging because particle insertion procedures are very inefficient in high density systems. We avoid this difficulty here by performing simulations in the canonical ensemble and calculating the Kirkwood-Buff integrals using a modified approach that is appropriate for this ensemble[12]. Instead of using eq. 1, we start by calculating the integral

$$G_{ij}(R) = \int_0^{2R} \left[f_{ij} g_{ij}^{NVT}(r) - 1 \right] 4\pi r^2 (1 - 3x/2 + x^3/2) dr, \tag{6}$$

which is the appropriate expression for finite-volume KB integrals[12]. In this expression, $x = r/(2R)$ and $g_{ij}^{NVT}(r)$ is the ra-

Max Planck Institute of Colloids and Interfaces, Theory and Bio-Systems Department, Wissenschaftspark Golm, 14424 Potsdam, Germany.
* E-mail: ana.vilaverde@mpikg.mpg.de, Fax: +49(0)331 567 9602; Tel: +49(0)331 567 9608.

dial distribution function in the NVT ensemble. The radial distribution function is identified in this section by the superscript NVT; in the remaining sections of this paper this superscript is dropped to simplify notation. f_{ij} is a concentration-dependent correction factor to the radial distribution function. This factor is necessary to correct the long range behavior of the radial distribution functions obtained from simulations in closed systems because these functions do not converge to unit at long distances, unlike those for open systems[3,13–15]. While there is no formal relation between $g_{ij}^{\mu VT}(r)$ and $g_{ij}^{NVT}(r)$,[13,16], prior work indicates that the ratio between $g_{ij}^{\mu VT}(r)$ and $g_{ij}^{NVT}(r)$ is of order $1 \pm 1/N$ where N is the number of particles in the system[13,14], i.e., for reasonably large systems such as those used here, the correction factor is small. The difference $G_{ij}(R) - G_{ij}$, between the integral calculated using equation 6 and the true integral calculated using equation 1, scales as $1/R$ for large values of R, so we obtain accurate estimates of the true value of the KB integral, G_{ij}, by linearly extrapolating $G_{ij}(R)$ to $1/R \to 0$. This approach has been successfully used to calculate Kirkwood-Buff integrals from simulations in the canonical ensemble[12].

1.2 Approach

In the original ion models, the Lennard-Jones interactions between anions and cations are obtained from Lorentz-Berthelot (LB) combination rules, and full, i.e., unscreened, electrostatic interactions are calculated between the Drude pairs associated with two ions. For $MgSO_4$, preliminary simulations (not shown) indicate that unscreened electrostatic interactions between the Drude pairs are inappropriate because they lead to unphysically short distances between Mg^{2+} and SO_4^{2-} ions in solution. For this reason, in the improved $MgSO_4$ model the short range electrostatic interactions between the Drude pairs associated with Mg^{2+} and with the oxygen atoms of SO_4^{2-} are screened. Introduction of the appropriate degree of screening is sufficient to reproduce the target activity derivative, so there is no need to alter the Lennard-Jones interactions between anions and cations in this case. The screened electrostatics between Mg^{2+} and SO_4^{2-} ions have a functional form originally introduced by Thole[17]:

$$U_{electr,Thole} = \frac{q_i q_j}{4\pi\varepsilon_0 r_{ij}} \left[1 - \left(1 + \frac{r_{ij}}{2a}\right)\exp(-r/a)\right] \qquad (7)$$

This functional form is selected because it is already used in the context of the SWM4-NDP water model, to screen the interactions between the Drude pairs of divalent cations and SWM4-NDP water[18], and is thus fully compatible with this model. In Equation 7, r_{ij} is the distance between the pair of charges of magnitude q_i and q_j, $a = \sqrt[6]{\alpha_i \alpha_j}/t_{ij}$ and $\alpha_{i,j}$ is the polarizability volume of the atoms associated with the i or j charges. The pairs of charges are those belonging to the Drude pairs of two ions whose interactions should be screened. For Mg^{2+} and SO_4^{2-} the Drude pairs are those associated with Mg^{2+} and with the sulfate oxygens (O_{sulf}): $q_i = \left\{q^{Mg^{2+}} - q_D^{Mg^{2+}}, q_D^{Mg^{2+}}\right\}$ and $q_j = \left\{q^{O_{sulf}} - q_D^{O_{sulf}}, q_D^{O_{sulf}}\right\}$. Here q^X without subscript denotes the total charge of the atom or ion X and q_D^X denotes the charge of the negative Drude particle belonging to X; $q^X - q_D^X$ thus indicates the core charge that co-localizes with the Lennard-Jones center of each atom or ion. t_{ij} is the dimensionless Thole screening parameter for the two particles being considered. This parameter determines the extent of screening between the two charges: for $t_{ij} \to 0$ the interactions are fully screened, for $t_{ij} \to \infty$ they are totally unscreened. The $t_{Mg,O_{sulf}}$ parameter is optimized in this study to reproduce the activity derivative of aqueous solutions of $MgSO_4$ with concentration 2.5 m.

Preliminary simulations (not shown) for CsCl indicate that screening the short range electrostatic interactions between the Drude pairs of Cs^+ and Cl^- increases the disagreement between the calculated solution activity derivative and the experimental value, so screening is not introduced for this salt. To reproduce the activity derivative of CsCl at 2.5 m, then, we instead optimize the energy parameter, $\varepsilon_{Cs,Cl}$, of the Lennard-Jones interactions between Cs^+ and Cl^-. These interactions are given by: $U_{LJ(r_{ij})} = \varepsilon_{ij}\left[\left(\frac{R_{min,ij}}{r_{ij}}\right)^{12} - 2\left(\frac{R_{min,ij}}{r_{ij}}\right)^{6}\right]$ where ε_{ij} and $R_{min,ij}$ are parameters that characterize the interactions between atoms i and j, and r_{ij} is the distance between these atoms. For all remaining Lennard-Jones interactions, the usual LB rule to calculate ε ($\varepsilon_{ij} = \sqrt{\varepsilon_{ii}\varepsilon_{jj}}$) applies. For all pairs of atoms including Cs^+ and Cl^-, $R_{min,ij}$ is calculated from the self-interaction parameters as usual: $R_{min,ij} = R_{min,ii}/2 + R_{min,jj}/2$.

1.3 Applying the Kirkwood-Buff theory to calculate activity derivatives for $MgSO_4$ and CsCl solutions

To parameterize the anion-cation interactions for $MgSO_4$ and CsCl we perform several production runs for each 2.5 m solution. All simulation details are given in the main text. Each run differs only in the value of the parameter to be optimized: $t_{Mg,O_{sulf}}$ or ε_{CsCl}. We test the values $t_{Mg,O_{sulf}} = 1.15, 1.178, 1.183, 1.2, 1.3$ for $MgSO_4$; for CsCl, we test $\varepsilon_{CsCl} = \lambda 0.1411$ kcal/mol, where 0.1411 kcal/mol is the ε_{CsCl} value in the original parameterization and $\lambda = 0.9, 1, 1.1, 1.2$. The $t_{Mg,O_{sulf}}$ are not evenly distributed because we opt to perform more simulations using $t_{Mg,O_{sulf}}$ values closer to the estimated optimum, for increased accuracy. These values of $t_{Mg,O_{sulf}}$ and ε_{CsCl} are selected from an initial set of simulations (not shown) that tested a wider range of values for both parameters. For each simulation we calculate the relevant radial distribution functions and start by examining their behavior at large inter-particle separations. This behavior is illustrated in Figure 1, which shows the long-range region of the anion-cation radial distribution functions for both salts and for the optimized values of $t_{Mg,O_{sulf}}$ and ε_{CsCl}. It is patent from the black and red lines in Figure 1 that correlations extend to much larger distances in $MgSO_4$ solutions than in CsCl ones: the $MgSO_4$ $g(r)$ shows oscillations as far as 30 Å whereas in the CsCl solution the $g(r)$ is essentially flat for $r > 20$ Å. Similar trends are observed for the anion-anion and cation-cation $g(r)$s (not shown). The grey lines in Figure 1 are the radial distribution functions for each of the 10 runs performed for each system. The large spread of these curves around the average over all simulations visually conveys the need to perform multiple runs for these systems. The ion-water radial distribution functions (not shown) are essentially flat at large distances indicating an absence of very long range ion-water correlations.

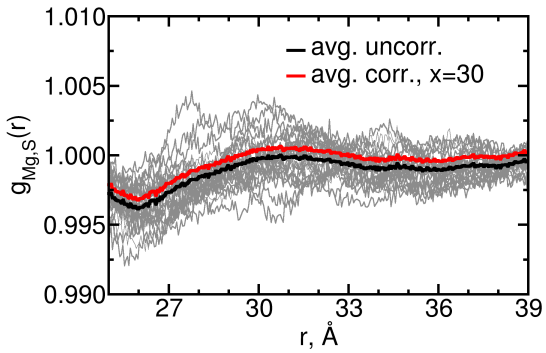

(a)

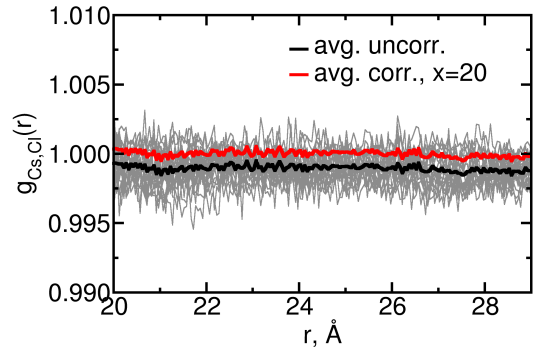

(b)

Fig. 1 Anion-cation radial distribution functions at 2.5 m, using the optimized anion-cation interaction parameters. The thin grey lines show the radial distribution function for each of the 10 production runs. The thick, labeled, lines show the radial distribution function averaged over all production runs, either uncorrected or corrected using an f_{ij} factor calculated according to Equation 8 using the indicated lower limit, x. (a) $MgSO_4$. (b) CsCl.

Figure 1 also illustrates that the radial distribution functions do not converge to unity at large distances, for the reasons mentioned above. We correct for this finite size effect by scaling each $g_{ij}(r)$ by a factor f_{ij} when calculating the KB integrals (see Equation 6). This factor is given by

$$f_{ij} = 1/\left\langle g_{ij}(r)\right\rangle_{r\in[x,L/2]}, \tag{8}$$

which is simply the inverse of the average $g_{ij}(r)$ in the interval $[x, L/2]$. The lower limit, x, is chosen so that for $r > x$ the radial distribution functions show only minimal oscillations and their values are already very close to unity; the upper limit is simply the maximum distance for which $g_{ij}(r)$ is calculated, i.e., half of the length of the simulation box. For $MgSO_4$, some of the radial distribution functions still show visible oscillations (of order ± 0.001) at separations comparable to half the simulation box size; these oscillations imply that the value of f_{ij} may depend on the lower limit used to calculate $\left\langle g_{ij}\right\rangle$. To evaluate the influence of the choice of lower limit on the calculated activity derivative, two values of x are tested for $MgSO_4$: $x = 27, 30$ Å. Solutions of CsCl show much smaller oscillations at large r, and so a single lower limit ($x = 20$ Å) is used to calculate the factors f_{ij}.

The Kirkwood-Buff integrals are calculated from the corrected radial distribution functions according to Equations 6 and 8, and the best estimate of G_{ij} is obtained by linearly extrapolating $G_{ij}(R)$ for $1/R \to 0$. This procedure is illustrated in Figure 2 for $G_{Mg,S}(R)$. Note that the estimate of G_{ij} obtained by linear extrapolation differs significantly from the last calculated value of $G_{ij}(R)$, indicating that the linear extrapolation step is indispensable to obtain good estimates of G_{ij}.

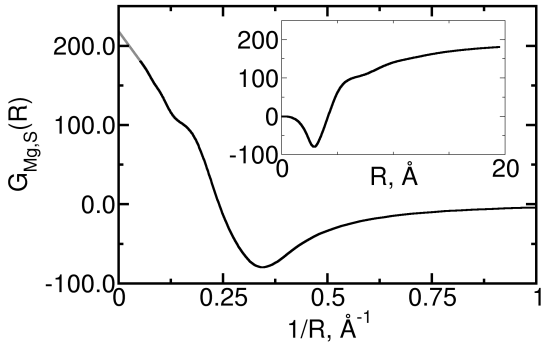

Fig. 2 Kirkwood-Buff integral, $G_{Mg,S}(R)$, for Mg^{2+} and SO_4^{2-} as a function of $1/R$, the inverse of half of the integration limit. The grey curve at small values of $1/R$ is the linear extrapolation when $R \to \infty$. The inset shows $G_{Mg,S}(R)$ as a function of R.

The activity derivative for each test value of the parameters $t_{Mg,O_{sulf}}$ and ε_{CsCl} is calculated according to Equation 5 from the G_{ij} estimates. These activity derivatives are shown in Figure 3. For $MgSO_4$ it is apparent that the solution activity derivative decreases markedly as the screening parameter increases, i.e., as the anion-cation electrostatic interactions become *less* screened. The statistical uncertainty of a_{cc} becomes significantly larger for lower values of $t_{Mg,O_{sulf}}$, a consequence of the slower solution dynamics observed for these systems. While it would be desirable to decrease this statistical uncertainty, this would have required simulation times even longer than those used in the present study, which was not possible with our resources. Since the values of a_{cc} for both lower thresholds used to calculate the correction factors f_{ij} are statistically indistinguishable, both values are used to estimate the $t_{Mg,O_{sulf}}$ value that should reproduce the experimentally determined a_{cc} for $MgSO_4$ solutions. In contrast to $MgSO_4$, the statistical uncertainty associated with the calculated a_{cc} for CsCl is quite small, consequence of the much faster solution dynamics of this aqueous solution which enables excellent sampling with our production run times. For both $MgSO_4$ and CsCl, the solution activity derivative depends linearly on the $t_{Mg,O_{sulf}}$ or ε_{CsCl} in the range of parameter values shown in Figure 3. We obtain the optimum values of $t_{Mg,O_{sulf}}$ and ε_{CsCl} by fitting a linear expression to all points in Figures 3(a) and 3(b) and then solving this expression against the experimental molar activity derivatives.

The optimized parameters for CsCl and $MgSO_4$ are given in Table 1. The molar activity derivatives of solutions of CsCl or $MgSO_4$

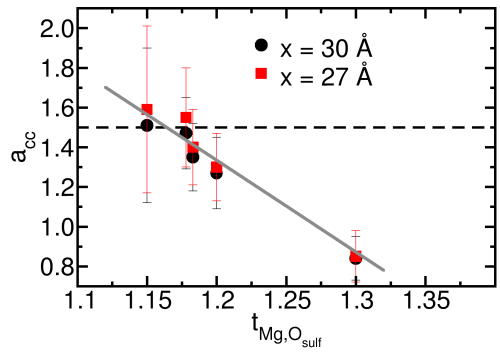

(a) MgSO4.

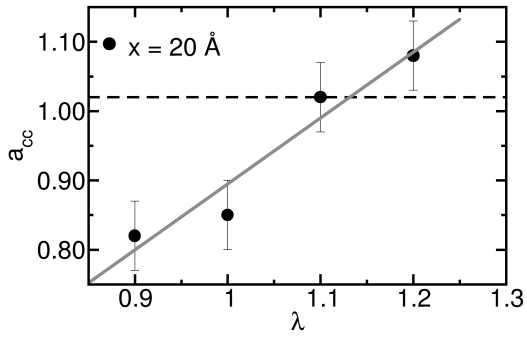

(b) CsCl.

Fig. 3 Molar activity derivative of 2.5 m solutions as a function of (a) $t_{Mg,O_{sulf}}$, for two different lower thresholds x of calculating the $g_{ij}(r)$ correction factors, f_{ij}; (b) The scaling factor λ for ε_{CsCl}. The error bars are obtained from block averages over five blocks, i.e., grouping two simulations into a block. The grey lines are linear fits to all points in each plot, the dashed black line indicates the experimental value of the activity derivative at this concentration.

of concentration 2.5 m calculated from new simulations using the final parameters are shown in Table 2. As expected, the activity derivative is close to the experimental value. The density of CsCl or $MgSO_4$ solutions at the three concentrations calculated from NPT simulations is shown in Table 3. The good agreement between the calculated and the experimentally measured density at all three concentrations, a property that was not used during the parameterization stage, lends confidence to our choice of force field. We emphasize that the ion-water interactions in the new

Table 1 Optimized anion-cation parameters for $MgSO_4$ and CsCl. See text for the definition of the parameters.

	Parameter	Value
CsCl	ε_{CsCl}	0.1603 kcal/mol
$MgSO_4$	$t_{Mg,O_{sulf}}$	1.161

CsCl and $MgSO_4$ models are unaltered, meaning that the new models reproduce properties of infinitely dilute solutions as well as the original models.

Table 2 Calculated and experimental molar solution activity derivatives for aqueous solutions of CsCl or $MgSO_4$ at 2.5 m. The sources of the experimental values are given in the third column.

	Calc.	Exp.	Ref.
CsCl	1.00±0.02	1.02	[4]
$MgSO_4$	1.4±0.1	1.5	[19]

Table 3 Calculated density of aqueous solutions of CsCl or $MgSO_4$ at 0.5, 1.5 and 2.5 m. The reference experimental values, given in parenthesis, are from the CRC Handbook[20].

	density (g/cm^3)	
conc. (m)	$MgSO_4$	CsCl
0.5	1.04 (1.06)	1.04 (1.06)
1.5	1.15 (1.16)	1.16 (1.18)
2.5	1.24 (1.26)	1.26 (1.28)

2 Induced dipole moments on sulfate anions by QM calculations

In this work, the Thole screening parameters for anion-cation pairs have been inferred via an indirect route, by empirically matching the experimental activity derivative to that determined from an auxiliary simulation. Given the time-consuming nature of this procedure, we also investigated the possibility of directly obtaining parameters of a Thole-like or anharmonic damping model from high-level quantum mechanical (QM) calculations. Considering that anions are usually far more susceptible to polarization than cations, we employed a numerical setup as shown in Figure 4(a), where the anion is placed in the electric field produced by a point-like test charge sufficiently far away. There are no additional orbitals associated with the test charge, hence an induced dipole moment can be computed unambiguously. Haibo *et al.* [18] used a similar setup for parameterizing the anharmonic damping of the induced dipole on a chloride anion. The electric field at the location of the anion was varied by varying the distance between the test charge and the chloride nucleus. While this appears to work well for small, single-atom anions, we found that the case of bulky anions such as SO_4^{2-} appears to be problematic. In Figure 4, we show a series of QM calculations where the dipole moment on a SO_4^{2-} ion is induced by a test charge $q_1 = +2e$. The electric field $|\vec{E}|$ at the position of the sulfur atom is varied by tuning the distance of the test charge between the two limits shown in the figure. Three different basis sets have been used: a standard correlation consistent set (cc-pVTZ) and an extension (aug-cc-pVTZ) including diffuse functions, as well as a corresponding Pople-style basis set (6-311++G(2df,2pd)) also comprising spatially extended orbitals (the same employed in ref. [18]). All calculations in the present work are of the single point type, and have been carried out at the HF and MP2 levels of theory, the results produced by both of them being in very close agreement. All computations were performed with the Gaussian software package[21].

Spatially extended (so called diffuse) orbitals may be expected to be essential in order to accurately model the outskirts of the electron density distribution, governing the anharmonic response

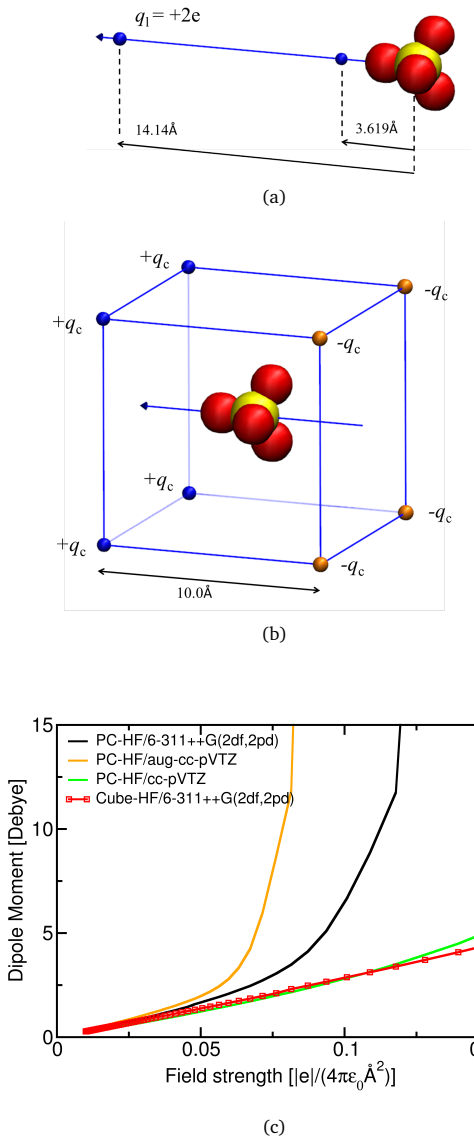

Fig. 4 Configurations used in the quantum mechanical calculations to infer the induced dipole moment on a SO_4^{2-} ion. In fig. 4(a) and 4(b), the positive $z-$direction is indicated by the arrow running through one the S–O bonds, with the sulfur placed at the origin. The electric field distribution around the ion is determined by point charges in two ways: (a) by placing a test charge q_1 along the $z-$axis at variable distances from the sulfur atom (extremal positions are indicated by blue spheres), and (b) by 8 point charges of equal magnitude q_c, placed at the corners of a cube of edge length 10, centered at the origin. The charges at the two opposing faces orthogonal to z are of opposite sign, as to generate a rather homogeneous electric field in the immediate vicinity of the SO_4^{2-} ion. The field strength $|\vec{E}|$ at the origin can be set by choosing $q_c = a^2|\vec{E}|3\sqrt{3}/64$. The graph in 4(c) displays the induced dipole moment on the anion as a function of the field strength at the origin for the line (PC) and the cube configuration (Cube). In the latter graph, red squares indicate the distribution of data points for the electric field.

of the anion. In Figure 4(c) we have compiled the variation of the dipole moment with electric field strength for the three basis sets in the single point charge configuration (Figure 4(a)) and the cube configuration (Figure 4(b)). It can be observed that all curves asymptotically agree on the dipole moment for weak fields. The use of diffuse basis sets (curves in orange and black) in combination with a divalent point charge quickly leads to a steep, unnatural increase of the dipole moment with increasing field strength, and the QM calculations become numerically unstable beyond $|\vec{E}| \sim 0.1\ |e|/(4\pi\varepsilon_0 m^2)$. Omitting the diffuse functions (green curve) brings the dipole moments very close to those obtained in the cube configuration of Figure 4(b) (red squares), independent of whether in the latter a diffuse or standard basis set is used. The cube configuration, emulating a rather homogeneous field distribution around the SO_4^{2-} ion, essentially results in a linear increase of the induced dipole moment.

The pronounced dependence of the dipole moment on the numerical setup is explained as follows. The strength of the electric field is specified as the value it attains at the location of the sulfur atom. Due to the spatial extent of SO_4^{2-}, the electric field is not constant across the ion, which experiences a field gradient. Even though the field strength at the origin may be moderate, at the oxygen closest to the test charge it is roughly a factor of 3 larger (for the closest approach), and the coulomb singularity leads to an artificial accumulation of electron density and hence to unrealistically large dipole moments. Similar artifacts occur in the cube configuration only for field strengths beyond $0.25\ |e|/(4\pi\varepsilon_0 m^2)$. Again, no regime seems to exist from which a damping behavior could be inferred.

Summarizing, for a simple setup with point-like test charges (and a rather bulky anion) in combination with diffuse basis sets, the behavior of the induced dipole moments is prone to show artifacts over the interesting range of distances between point charge and anion. Omitting diffuse functions, on the other hand, does not produce the expected damping of the dipole moment and numerical instabilities are only shifted towards higher field strengths. It appears rather difficult and unreliable to *tune* the theory level in combination with a setup of point-like test charges in order to reproduce the expected effects. In fact, with respect to a quantum chemical approach one should resort to *ab initio* molecular dynamics in explicit solvent, to include effects such as screening, charge transfer and possibly modified anion polarizabilities in a condensed phase environment[22]. This, however, requires an accurate and unambiguous assignment of charge density to each of the ionic species involved[23], which is beyond the scope of the present work.

3 Water reorientation in $MgSO_4$ and CsCl solutions

As mentioned in the main text, the average water reorientation decay in $MgSO_4$ and CsCl solutions is non-exponential for $t < 200$ fs, and is well-described by a sum of two exponentials for $t > 200$ fs. The behavior at $t < 200$ fs, while non-exponential, can be approximated as an exponential, so that the full reorientation decay can be well-fit by a sum of three exponentials: $a\exp(-t/\tau_1) + b\exp(-t/\tau_2) + c\exp(-t/\tau_3)$. An average reorientation time can be calculated from the results of the fit as $\tau_{rot} = (a\tau_1 + b\tau_2 + c\tau_3)/(a+b+c)$, similarly to what was done for water subpopulations near isolated pairs or clusters of ions. In Table 4

we show the results of this fit and the average reorientation times for water in solutions of $MgSO_4$ or CsCl.

Table 4 Fitting constants and average reorientation decay times (ps) for water molecules in $MgSO_4$ and CsCl solutions. See text for further details.

salt	$MgSO_4$			CsCl		
conc. (m)	2.5	1.5	0.5	2.5	1.5	0.5
a	0.229	0.245	0.265	0.245	0.256	0.262
t_1 (ps)	0.091	0.095	0.100	0.093	0.097	0.098
b	0.199	0.275	0.315	0.237	0.234	0.200
t_2 (ps)	1.193	1.137	1.020	0.810	0.823	0.735
c	0.573	0.480	0.421	0.518	0.510	0.538
t_3 (ps)	10.188	6.346	3.447	2.803	2.547	2.222
τ_{rot} (ps)	6.1	3.4	1.8	1.7	1.5	1.4

4 Anion-cation radial distribution function

The position and intensity of the extrema of the anion-cation radial distribution function for CsCl and $MgSO_4$ solutions is given in Table 5. The absence of contact ion pairs (CIPs) and the presence of solvent-shared and solvent separated ion pairs in $MgSO_4$ solutions is supported by results from Raman spectroscopy[24,25], calorimetric studies[26,27] and early ultrasonic relaxation measurements[28]. The Raman studies, done at concentrations of about 2 M, show that the spectrum of SO_4^{2-} is not affected by the presence of Mg^{2+}, which is consistent with the absence of CIPs. The calorimetric studies indicate that the partial molal entropies of metal sulfate ion pairs are negative for $MgSO_4$ and $ZnSO_4$, suggesting formation of SIPs, but positive for Cs_2SO_4 and $CaSO_4$, consistent with the formation of CIPs and the release of water molecules from the hydration shells of the ions. The Thz/FIR measurements, done at concentrations up to the solubility limit, show low frequency mode distributions; accompanying calculations indicate that results are explained by the presence of SIPs and 2SIPs only. We point out, however, that other experiments have suggested that CIPs are present in $MgSO_4$ solutions. For example, Raman spectroscopy up to 2.5 M, ultrasonic measurements up to 0.2 M and dielectric relaxation spectroscopy up to 2.5 M suggest that Mg^{2+} and SO_4^{2-} form CIPs even at low salt concentrations[29–32]. The interpretation of the dielectric relaxation measurements, however, relies strongly on the assignment of relaxation times of order 30 ps to the contact ion pair. As we show below, relaxation times of this magnitude arise for water molecules directly between ions forming a solvent-shared ion pair, raising the possibility of reinterpreting the existing dielectric relaxation data.

Table 5 Maxima and minima of the uncorrected anion-cation radial distribution functions for 2.5 m solutions of $MgSO_4$ or CsCl. For $MgSO_4$, the $g(r)$ is calculated using the sulfur atom. Data obtained by fitting gaussian curves to the extrema; the uncertainty of each value is the asymptotic error of each fit.

Salt	Extremum	r, Å	g(r)
$MgSO_4$	max_1	5.011 ± 0.003	4.99 ± 0.05
	min_1	5.328 ± 0.003	2.83 ± 0.01
	max_2	5.577 ± 0.002	3.38 ± 0.01
	min_2	6.390 ± 0.003	0.606 ± 0.002
	max_3	7.433 ± 0.004	1.216 ± 0.001
	min_3	8.718 ± 0.003	0.6383 ± 0.0003
CsCl	max_1	3.565 ± 0.003	5.16 ± 0.03
	min_1	4.534 ± 0.002	0.8993 ± 0.0008
	max_2	5.420 ± 0.003	1.438 ± 0.001
	min_2	6.840 ± 0.003	0.9281 ± 0.0007

In contrast to $MgSO_4$, the anion-cation radial distribution functions for CsCl solutions have only two peaks, the first one corresponding to contact ion pair and the second to solvent-shared configurations. These findings are consistent with the limited experimental information available for this salt. Dielectric relaxation spectroscopy[33,34], infra-red attenuated total reflection spectroscopy[35,36] and analysis of freezing point depression measurement's[37] indicate that CsCl forms weak ion pairs in aqueous solutions of a wide range of concentrations, but the nature of the ion pairs could not be identified from these measurements. The type of ion pairs formed by CsCl could be identified from recent electric conductivity measurements at concentrations < 0.005 mol/dm^3, together with a two-dimensional model for water and ions parameterized to reproduce the association constants obtained from those measurements: CsCl forms both weak CIPs and SIPs[38], consistent with our simulation results. New analyses[38,39] of early conductivity data[40] are also in line with these results.

The distribution of the probability of forming various numbers of ion pairs per ion in $MgSO_4$ solutions of concentration 2.5 m is shown in Figure 5. At this concentration, most ions participate in 4 or 5 ion pairs, indicating that clusters are frequent. The abundance of clusters in concentrated $MgSO_4$ solutions is consistent with the large supra-additive slowdown visible in these solutions, shown in the main text to originate in ion clusters.

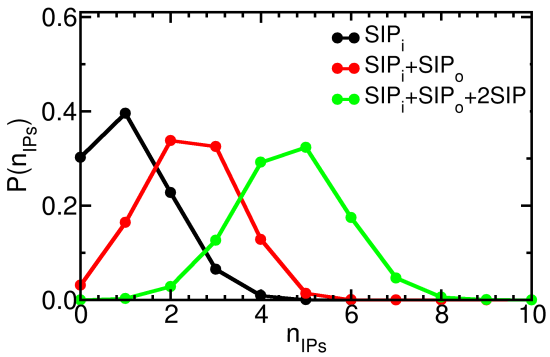

Fig. 5 Probability per ion of forming $0, 1, 2, \cdots$ ion pairs of the indicated types in $MgSO_4$ solutions of concentration 2.5 m.

5 Calculation of ion pair lifetimes

We calculate ion pair lifetimes using the stable states framework developed by Northrup and Hynes[41], as implemented by Joung and Cheatham[42]. In this framework, only transitions between stable ion pair configurations are considered in the calculation

of the lifetime; transient events where the ion pairs breakup and quickly reform are disregarded. This is achieved by defining stable reactant and product states from the positions of the extrema of the anion-cation radial distribution functions. A complete ion pair state, signaled by a maximum i in the anion-cation $g(r)$, is delimited simply by the positions of the minima i to its left (if it exists) and $i+1$ to its right. A stable ion pair state, however, considers only the subset of configurations closer to the maximum i: the left and right boundaries of each stable ion pair state associated with maximum i in the $g(r)$ are the distances satisfying the conditions $\sqrt{g(r_{min,i})g(r_{max,i})}$, if minimum i exists, and $\sqrt{g(r_{max,i})g(r_{min,i+1})}$. To calculate the ion pair lifetime, we consider only transitions between stable ion pair states, and compute the survival function $S(t)$:

$$S(t) = \langle n_R(0) n_R(t) \rangle \tag{9}$$

In this expression $n_R(0) = 1$ when an anion and a cation form a stable ion pair at time 0 (i.e, a reactant pair); $n_R(0) = 0$ otherwise. $n_R(t) = 1$ up to the instant, t, when the original reactant pair forms a different, stable (i.e, product), ion pair; $n_R(t) = 0$ from that time onwards, even if the original reactant state reforms. The average is over all $n_R(0) = 1$. The calculated survival functions (not shown) are well-fitted by a monoexponential $\exp(-t/\tau_{IP})$, from which the ion pair lifetimes, τ_{IP}, shown in the main text, are obtained. The inner and outer SIPs seen in $MgSO_4$ solutions are considered a single state for the purpose of the lifetime calculation.

5.1 Explaining the differences between ion pair lifetimes in CsCl and $MgSO_4$ solutions

For CsCl, the ion pair lifetimes are primarily governed by diffusion: all ion pair lifetimes at all concentrations are comparable to the time, τ_D, it takes each ion to diffuse over 1 Å, half of the distance necessary to break an ion pair: τ_D=7 ps. For example, the CIP lifetime is 6.7 ps and the SIP lifetime is 4.6 ps at 0.5 m. The shorter SIP lifetimes relative to the CIP ones can be explained by the fact that there are two pathways to break a SIP – the ions can either move closer together to form a CIP or they can move even further apart – whereas CIPs may break only by forming a SIP.

We also examine the possibility that the differences between SIP and CIP lifetimes in CsCl solutions could reflect differences in the magnitude of the anion-cation electrostatic interactions in each ion pair configuration. We do so by calculating the electrostatic energy, U, between two charges of magnitude ± 1 |e| in a medium of dielectric constant 78 at the characteristic CIP and SIP distances. $U = -2.0$ k_BT (T=300 K; k_B is Boltzmann's constant) for a charge-charge distance $D = 3.6$ Å, corresponding to a CsCl CIP, and $U = -1.4$ k_BT for $D = 5$ Å, corresponding to a CsCl 2SIP. The difference $\Delta U = -1.4 + 2.0 = 0.6$ k_BT must be supplied to break a CIP; this small difference indicates that, for CsCl, the electrostatic anion-cation electrostatic interactions do not govern the ion pair lifetimes.

The lifetimes of $MgSO_4$ 2SIPs also appear to be governed primarily by diffusion: for example, the 2SIP lifetime is 24 ps at 0.5 m, and $\tau_D = 20$ ps at the same concentration. At 2.5 m, the 2SIP lifetime is 53 ps and the $\tau_D = 70$ ps. The magnitude of the electrostatic anion-cation interactions (calculation not shown) indicates that these interactions should not significantly influence the 2SIP lifetimes.

The lifetimes of $MgSO_4$ SIPs, however, are much longer than τ_D, indicating that something other than diffusion is governing their breakage. For example, at 0.5 m, $\tau_D = 20$ ps and the SIP lifetime is 118 ps. To assess the contribution of the ion valence to the SIP lifetime, we compare the electrostatic energy between two charges of magnitude ± 2 |e| in a medium of dielectric constant 78 at characteristic ion pair distances. $U = -5.7$ k_BT for a charge-charge distance $D = 5$ Å, corresponding to a $MgSO_4$ SIP_i, and $U = -3.8$ k_BT for $D = 7.5$ Å, corresponding to a $MgSO_4$ 2SIP. Breaking a SIP_i thus requires at least $\Delta U = -3.8 + 5.7 = 1.9$ k_BT; for comparison, breaking a 2SIP pair by increasing the anion-cation distance by 2 Å requires only 0.3 k_BT. The difference in the electrostatic energy necessary to break SIP and 2SIP pairs and the differences between their lifetimes suggest that the large lifetimes of $MgSO_4$ SIP pairs are caused by the strong electrostatic attraction between ions in SIP configuration: if we assume that the time required to further separate the ions in a 2SIP pair can be written as $\tau_{2SIP} \times 2 = 24 \times 2 = k \times \exp(+\beta 0.3)$ – i. e., we consider an uphill free energy landscape associated with this process; the factor of 2 is there because 2SIP can break both by shortening or lengthening the anion-cation distance, and here consider only the latter possibility; k is a constant related to diffusion; then $\tau_{SIP} = 118$ ps is consistent with an uphill energy difference of 1.2 k_BT, which is comparable to the electrostatic $\Delta U = 1.9$ k_BT.

All ion pair lifetimes are necessarily dependent on the structure of water around the ions and on the time scales of its reorganization. This water structure will introduce a free energy barrier between ion-pair configurations, something that the simplistic analysis presented above does not include. Despite this obvious limitation of the arguments presented above, these arguments are sufficient to largely explain the trends observed in the ion pair lifetimes of CsCl and $MgSO_4$ solutions.

6 Water reorientation near isolated ions

We use the $P_2(t)$ function defined in the main text to quantify the OH reorientation dynamics in the vicinity of isolated ions (i.e., from the isolated ion simulations). Water subpopulations are partitioned in two different manners around the isolated ions: (i) We consider water subpopulations corresponding to the ions' first or second hydration layers, where the boundaries of each layer are the minima in the ion-water oxygen radial distribution function; the ion-water oxygen radial distribution functions can be found in our prior publication[43]. The reorientation decay of each hydration layer is shown in Figure 6; the corresponding average reorientation decay times, calculated as described in the main text, are shown in Table 6. These reorientation decays are used as input to the analytical model described by Equation 2 in the main text. (ii) We consider waters in spherical shells with mid-point distance d to the ions and thickness 1 Å; the corresponding average reorientation times, calculated as described in the main text, are shown in Table 7. The average reorientation times shown in Table 7 are

used in the calculation of the cooperative factor, S, around ion pairs or clusters. The reorientation times calculated according to (i) and (ii) are similar because both definitions capture similar water subpopulations.

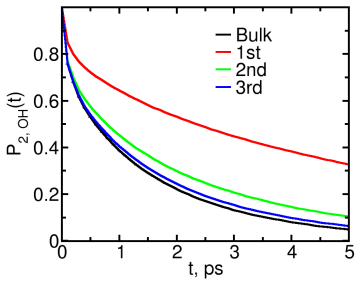

(a) Mg^{2+}.

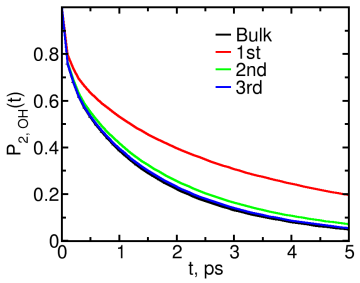

(b) SO_4^{2-}.

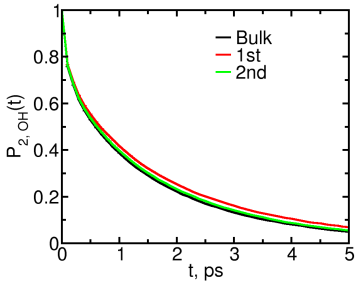

(c) Cs^{+}.

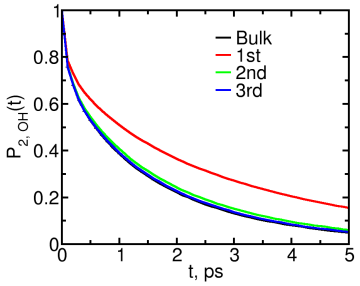

(d) Cl^{-}.

Fig. 6 $P_2(t)$ function calculated for water hydroxyl groups for waters belonging (at t=0) to the indicated hydration layers around isolated ions. For comparison, the reorientation decay of pure water is also shown.

Table 6 Average OH reorientation times (ps) of waters with oxygen atoms belonging (at t=0) to the first or second hydration layers (HLs) of the indicated isolated ions.

ion	1st HL	2nd HL
Mg^{2+}	4.7	1.8
SO_4^{2-}	2.8	1.5
Cs^{+}	1.5	1.3
Cl^{-}	2.3	1.4

Table 7 Average OH reorientation times (ps) of waters with oxygen atoms belonging (at t=0) to spherical shells with thickness 1 Å and mid-point distance d to the indicated isolated ions.

d (Å)	Mg^{2+}	SO_4^{2-}	Cs^{+}	Cl^{-}
2	4.7	–	–	–
3	–	2.6	1.5	2.5
4	1.9	2.9	1.4	1.4
5	1.6	1.6	1.4	1.5
6	1.5	1.5	1.3	1.4
7	1.4	1.4	1.3	1.3
8	1.3	1.4	1.3	1.3

7 Low charge density cations affect dynamics of water around anions

We note that the Cs^{+} cation, which when isolated slows down water dynamics only minimally, seems to induce a sizable extra slowdown of water in the first hydration layer of Cl^{-} when forming a solvent-shared ion pair. Polarization-resolved femtosecond infrared pump-probe spectroscopy measurements of solutions of various 1:1 salts at frequencies that select for water hydroxyl groups hydrogen bonded to the anion – and largely leave out water hydroxyl groups hydrogen bonded to other water molecules – have suggested that the reorientation dynamics of these groups depends on the nature of the counterion, with the magnitude of this effect increasing with the charge density of the ions[44,45]; similar trends have been found using 2D IR vibrational echo spectroscopy[46] . Our results are consistent with that scenario and suggest such effects may occur already for low charge density ions such as Cs^{+}. In the main text, however, we show that the average water dynamics in CsCl solutions could be understood as the sum of contributions of water dynamics near isolated ions and water considered in bulk conditions, which apparently contradicts the combined effect of anions and cations observed in simulations of fixed $Cs^{+}\cdots Cl^{-}$ ion pairs and experimental observation. This contradiction can be lifted if one considers that the magnitude of the extra slowdown of water rotation by ion pairs relative to that induced by isolated ions is small – the maximum increase in the reorientation time constants is 1 ps – and the fraction of water molecules affected is also small. In other words, we expect the extra slowdown of water rotation brought by the presence of ion pairs to not be noticeable when considering the overall water dynamics in solution.

8 Reorientation decay times and cooperativity factors

The average reorientation times and cooperativity factors for water OH groups around ion configurations with fixed anion-cation distances and freely rotating ions not displayed in the main text are shown in Figures 7 and 8.

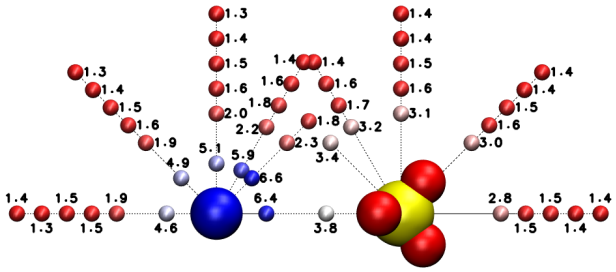

(a) $MgSO_4$ ion pair, 2SIP configuration.

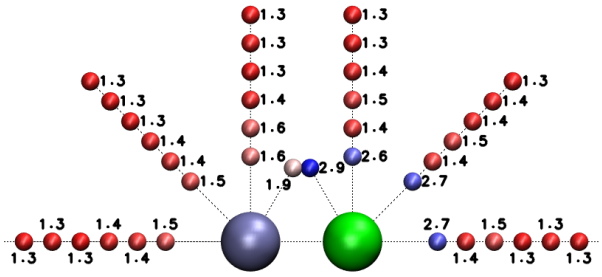

(b) CsCl ion pair, CIP configuration.

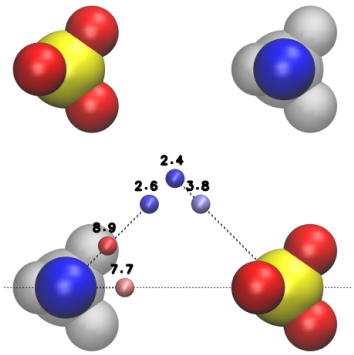

(c) $MgSO_4$ cluster, 2SIP configuration.

Fig. 7 Average reorientation decay times (ps) of OH groups belonging to different water subpopulations around the indicated ion aggregates. The color scale of the smaller spheres conveys, for each panel, the magnitude of the reorientation time shown next to the spheres. Consecutive water subpopulations along the dashed lines are 1 or 2 Å apart. The subpopulations closest to Mg^{2+} are at $d = 2$ Å and those closest to SO_4^{2-} at $d = 4$ Å.

9 Water reorientation dynamics in concentrated $MgSO_4$ solutions as the sum of contributions of water subpopulations near ion pairs

We assume that all ion pairs in solution can be considered isolated, and estimate the average water reorientation dynamics

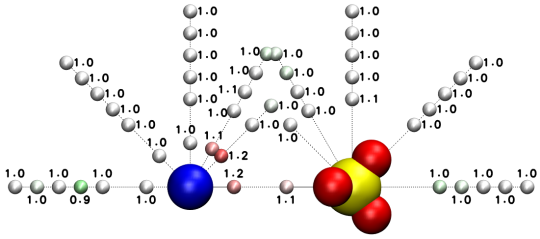

(a) $MgSO_4$ ion pair, 2SIP configuration.

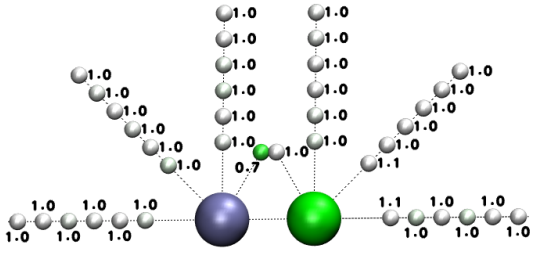

(b) CsCl ion pair, CIP configuration.

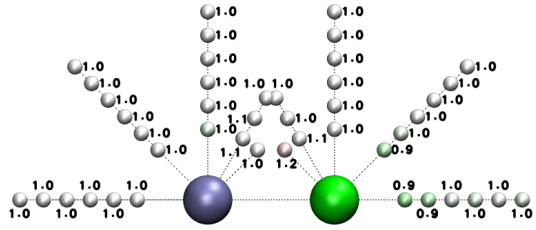

(c) CsCl ion pair, SIP configuration.

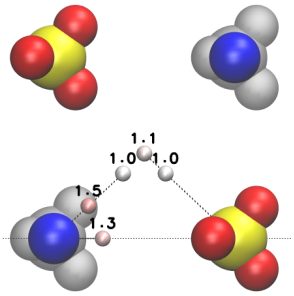

(d) $MgSO_4$ cluster, 2SIP configuration.

Fig. 8 Cooperativity factor of OH groups belonging to different water subpopulations around the indicated ion aggregates. The color scale of the smaller spheres conveys, for each panel, the magnitude of he cooperative slowdown factor shown next to the spheres. Consecutive water subpopulations along the dashed lines are 1 or 2 Å apart. The subpopulations closest to Mg^{2+} are at $d = 2$ Å and those closest to SO_4^{2-} at $d = 4$ Å.

in $MgSO_4$ solutions as the sum of the contributions of water molecules near ion pairs and those under bulk conditions, if they exist, according to the expression

$$P_{2,solution}(t) = \frac{n_b}{n_w} P_{2,b}(t) + \sum_{i=1}^{3} \frac{n_{pairs,i}}{n_w} \sum_{j=1}^{4} n_{w,j,i} P_{2,j,i}(t) \qquad (10)$$

In this expression, water molecules are partitioned between the three different types of ion pairs, indicated by the subscript i (inner or outer SIP, or 2SIP, respectively $i = 1, 2, 3$). For each ion pair,

four different water subpopulations, denoted by the subscript j, may be considered. The number of water molecules in each subpopulation near the ions is indicated by $n_{w,j,i}$ and their reorientation dynamics by $P_{2,j,i}$; n_b and $P_{2,b}(t)$ are the analogous quantities for water molecules considered in a bulk environment. n_w is the total number of water molecules in the simulation of the salt solution and $n_{pairs,i}$ is the total number of ion pairs of type i formed in the solution. The subpopulations included to model the solution reorientation dynamics at each concentration depend on the total number of ion pairs formed per ion at that concentration. At all concentrations, waters within a cylindric region lying between the two ions are included in the model. At the lowest concentration, each ion participates in less than two ion pairs, so we consider also waters belonging to the ionic half-spheres that cap that cylinder. At 1.5 m and 2.5 m, each ion participates in more than two ion pairs so the half spheres are no longer necessary; in this case, however, the model must include the water subpopulation within a second cylinder, which forms a 90° angle with the first one. This cylinder is called *excluded* because it contains only those water molecules which are not included in the first cylindric region. The terms in the model are used in order decreasing perturbation of water dynamics: water molecules are assigned to the cylinders of the SIP_i, followed by the cylinders of the SIP_o and 2SIPs, and only afterwards to the SIP half-spheres for the lowest concentration, or to the SIP_o and 2SIP excluded cylinders, at the other concentrations. Water molecules with bulk-like dynamics are only assumed to exist at the two lowest concentrations[46]. The results of this model depend on the radius considered in the definition of the water subpopulations around the cation and the anion, so several values for these radii were tested within physically reasonable limits. The results presented in the main text correspond to the best agreement between the analytical model and the reorientation decay measured directly in the simulations of salt solutions At 2.5 m, all water subpopulations were defined by a radius R=4 Å, which is intermediate between the first hydration layer of the cation (3.02 Å) and the anion (4.65 Å); at 1.5 m, R=4.65 Å; at 0.5 m, the radius of the anionic half-sphere and the cylinder are R=4.65 Å and the radius of the cationic half-sphere is R=5.01 Å, the limit of the second hydration layer of the cation.

10 Water reorientation dynamics in concentrated $MgSO_4$ solutions as the sum of contributions of water subpopulations near ion clusters

We assume that all ions in $MgSO_4$ solutions form static, isolated, cubic clusters, and estimate the reorientation dynamics in $MgSO_4$ solutions according to the expression

$$P_{2,solution}(t) = \frac{n_b}{n_w} P_{2,b}(t) + \frac{n_+}{n_w} \sum_{k=1}^{3} \frac{n_k}{n_p} \sum_{j=1}^{3} n_{w,j,k} P_{2,j,k}(t) \qquad (11)$$

In this expression, water molecules are partitioned between the three different types of ion clusters, indicated by the subscript k (inner or outer SIP, or 2SIP, respectively $k = 1,2,3$). For each ion cluster, three different water subpopulations, denoted by the subscript j, may be considered: the hydration shells of the anions, the cations, and the water in the central region of the cube that does not belong to the hydration shells. The number of water molecules per ion in each subpopulation near the ions is indicated by $n_{w,j,k}$ and their reorientation dynamics by $P_{2,j,k}$; n_b and $P_{2,b}(t)$ are the analogous quantities for water molecules considered in a bulk environment. The subpopulations included to model the solution reorientation dynamics at each concentration depend on the total number of ion pairs formed per ion at that concentration. For both the 1.5 and 2.5 m concentrations, waters are distributed between the anionic and cationic hydration shells according to the relative abundance of the three different types of ion pairs, and then to the central region of the 2SIP cube*. The remaining water molecules at 1.5 m are assigned bulk-like dynamics; at 2.5 m, the bulk-like term in Equation 11 is not used. n_w is the total number of water molecules in the simulation of the salt solution, n_+ is the total number of cations or anions in the solution; n_k is the number of ion pairs of each type formed per ion (i.e., the data shown in Table 2 in the main text) and n_p is the total number of ion pairs formed per ion ($n_p = n_{SIP_o} + n_{SIP_i} + n_{2SIP}$, shown in Table 2 in the main text).

The results of this model depend on the radius considered in the definition of the water subpopulations around the cation and the anion, so several values for these radii were tested within physically reasonable limits. The results presented in the main text correspond to the best agreement between the analytical model and the reorientation decay measured directly in the simulations of salt solutions. The results for the 1.5 m concentration correspond to a radius of 4.65 Å (the limits of the first hydration layer of SO_4^{2-}) for both the anion and the cation water subpopulations; for the 2.5 m concentration, the same radius was used for the anion; for the cation, a radius of 3.02 Å (the boundary of the first hydration layer of Mg^{2+}) was used.

11 Correlation between electric field characteristics and water slowdown for region C in $MgSO_4$ pairs

As mentioned in the main text, water subpopulations not belonging to Mg^{2+}'s first hydration shell in isolated $MgSO_4$ ion pairs with freely rotating SO_4^{2-} show reorientation slowdown that correlates with increased electric field magnitude. This correlation can be seen in Figure 9.

12 Correlation between electric field and water dynamics in SIP_i ion pairs with fixed SO_4^{2-} orientation

We investigate the surprising absence of a strong correlation between the characteristics of the local electric fields and OH rotation more deeply, by explicitly examining the dependence of water reorientation near ion pairs on sulfate orientation and dipole moment. We perform additional simulations of $MgSO_4$ ion pairs

* The anionic and cationic shells of the SIP cubic clusters already include all the water molecules in the central region of those cubes.

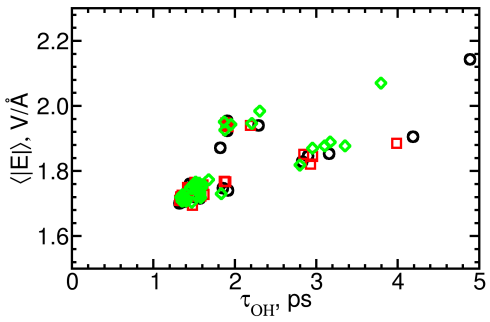

Fig. 9 Electric field magnitude, $\langle|\vec{E}|\rangle$ as a function of the reorientation time of water OH groups belonging to different water subpopulations around $MgSO_4$ SIP_i, SIP_o and 2SIP with freely rotating ions and outside Mg^{2+}'s first hydration shell (i.e, region C as defined in the main text).

in SIP_i configuration, where both ion orientation and dipolar moment take the fixed values shown in Table 8. We perform a total of six simulations based on two sulfate configurations, one where the SO_4^{2-} dipole moment, $|\vec{p}| = 0.26$ |e|Å, has the same value as the average $|\vec{p}|$ in the SIP_i simulations with freely rotating ions discussed in the prior sections and in the main text and, for comparison, another configuration where $|\vec{p}| = 0.22$ |e|Å, the average dipole moment of sulfate in water at infinite dilution‖. For each SO_4^{2-} configuration we perform simulations with three different SO_4^{2-} orientations so that the component of the dipole moment along the anion-cation direction, p_z, is either +0.14, 0 or -0.14 |e|Å; $p_z = +0.14$ |e|Å is the average p_z in the SIP_i simulations with freely rotating SO_4^{2-}. For each simulation, we calculate

Table 8 Details of simulations of $MgSO_4$ SIP_i pairs with fixed anion-cation distance and fixed SO_4^{2-} orientation. $|\vec{p}|$ is the magnitude of the SO_4^{2-} dipole moment and $|\vec{p}_z|$ the component of the SO_4^{2-} dipole moment along the anion-cation direction

$\|\vec{p}\|$, |e|Å	$\vec{p}_z$, |e|Å
0.22	+0.14
0.22	0
0.22	-0.14
0.26	+0.14
0.26	0
0.26	-0.14

the average OH reorientation time, the average reorientation time of the electric field and its average magnitude as a function of water subpopulation as described in the main text for the case of ion pairs with freely rotating ions. The spatial distributions of the average OH reorientation times are shown in Figures 10 and 11, and the correlation between these reorientation times and the average magnitude of the electric field in each water subpopulation is shown in Figure 12. Figure 12 shows that water rotation near ion pairs with fixed ion orientation correlates with the magnitude of the electric field similarly to the freely rotating ion pairs (see main text), indicating that simulations where the ions are not free to rotate may be used to gain insight into the mechanisms leading to supra-additive slowdown.

Figures 10 and 11 show that the magnitude of supra-additive slowdown observed in these simulations is strongly a function of the specific SO_4^{2-} configuration and orientation used, but shows no strong correlation with either the total magnitude of the SO_4^{2-} dipole moment or the magnitude of its dipole moment along the anion-cation direction. For example, supra-additive slowdown similar to that occurring in a SIP_i ion pair with freely rotating ions is observed for three simulations where both the average dipole moment and its component along the anion-cation direction differ markedly: those simulations with $(\vec{p}, \vec{p}_z) = (0.26, +0.14)$, $(0.22, 0)$ and $(0.22, -0.14)$ |e|Å. The ion pair with $(\vec{p}, \vec{p}_z) = (0.22, +0.14)$ |e|Å, which has a less intense SO_4^{2-} dipole moment, shows much stronger cooperative slowdown than that with $(0.26, +0.14)$ |e|Å, which has a larger dipole moment but similar $\vec{p}_z$. These results suggest that the extra forces, $\vec{f}_{p12}$, acting on the rotating water molecules because of the polarizability of the ions are weakly related, at best, to the supra-additive slowdown detected near $MgSO_4$ SIP_i ion pairs.

References

1 J. G. Kirkwood and F. P. Buff, *J. Chem. Phys.*, 1951, **19**, 774–777.
2 P. G. Kusalik and G. N. Patey, *J. Chem. Phys.*, 1987, **86**, 5110–5116.
3 M. Fyta and R. R. Netz, *J. Chem. Phys.*, 2012, **136**, 124103–11.
4 M. B. Gee, N. R. Cox, Y. Jiao, N. Bentenitis, S. Weerasinghe and P. E. Smith, *J. Chem. Theory Comput.*, 2011, **7**, 1369–1380.
5 B. Klasczyk and V. Knecht, *J. Chem. Phys.*, 2010, **132**, 024109.
6 S. Weerasinghe and P. E. Smith, *J. Chem. Phys.*, 2003, **119**, 11342–11349.
7 R. Chitra and P. E. Smith, *J. Phys. Chem. B*, 2002, **106**, 1491–1500.
8 S. Weerasinghe and P. E. Smith, *J. Chem. Phys.*, 2003, **118**, 10663–10670.
9 D. Horinek and R. R. Netz, *J. Phys. Chem. A*, 2011, **115**, 6125–6136.
10 D. G. Hall, *Trans. Faraday Soc.*, 1971, **67**, 2516–2524.
11 K. E. Newman, *Chem. Soc. Rev.*, 1994, **23**, 31–40.
12 P. Krueger, S. K. Schnell, D. Bedeaux, S. Kjelstrup, T. J. H. Vlugt and J.-M. Simon, *J. Phys. Chem. Let.*, 2013, **4**, 235–238.
13 T. L. Hill, *Statistical Mechanics- principles and selected applications*, Dover, 1987.
14 J. L. Lebowitz and J. K. Percus, *Phys. Rev.*, 1961, **122**, 1675–1691.
15 A. P. Lyubartsev and S. Marcelja, *Phys. Rev. E*, 2002, **65**, 041202–.
16 J. D. Ramshaw, *Mol. Phys.*, 1980, **41**, 219–227.
17 B. Thole, *Chem. Phys.*, 1981, **59**, 341–350.

‖ The average dipole moment of sulfate in water is not zero because hydrogen-bonding with water polarizes the ion in a non-spherically symmetric way.

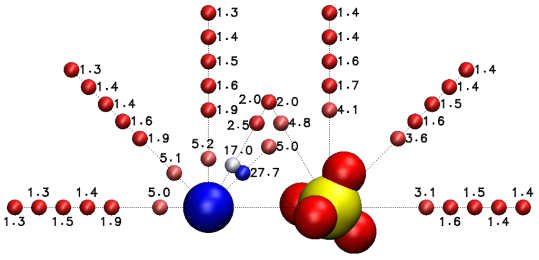

(a) $(\vec{p},\vec{p}_z)=(0.22,+0.14)$ $|e|$Å

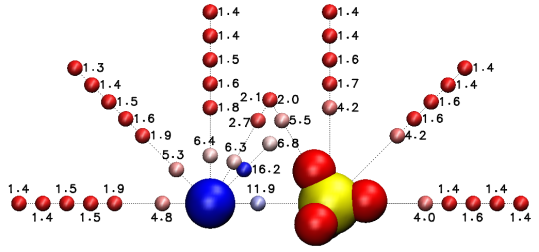

(b) $(\vec{p},\vec{p}_z)=(0.22,0)$ $|e|$Å

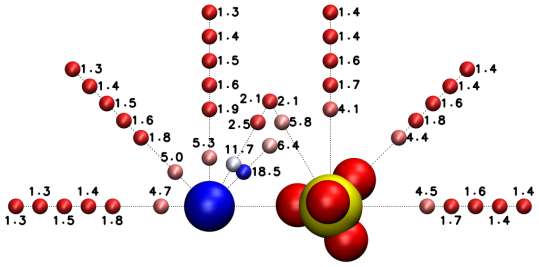

(c) $(\vec{p},\vec{p}_z)=(0.22,-0.14)$ $|e|$Å

Fig. 10 Average reorientation decay times (ps) of OH groups belonging to different water subpopulations around $MgSO_4$ SIP_i ion pairs with fixed ion configuration and orientation. The color scale of the smaller spheres conveys, for each panel, the magnitude of the reorientation time shown next to the spheres. Consecutive water subpopulations along the dashed lines are 1 or 2 Å apart. The subpopulations closest to Mg^{2+} are at $d=2$ Å and those closest to SO_4^{2-} at $d=4$ Å. The subpopulations at $(Mg^{2+},2Å,0^\circ)$ are only shown when they are sufficiently large to allow a good-quality fit to the $P_2(t)$ curve.

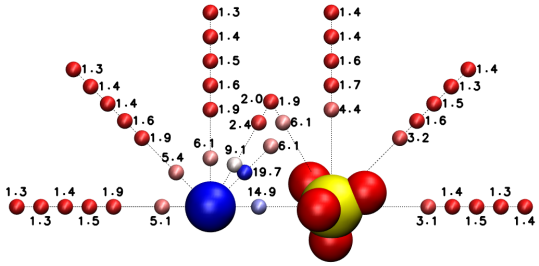

(a) $(\vec{p},\vec{p}_z)=(0.26,+0.14)$ $|e|$Å

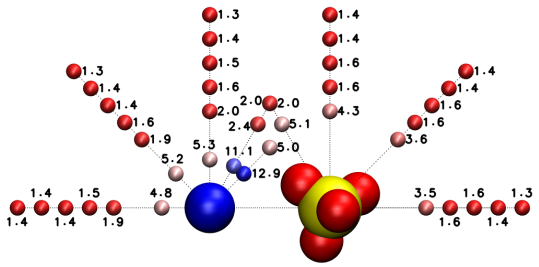

(b) $(\vec{p},\vec{p}_z)=(0.26,0)$ $|e|$Å

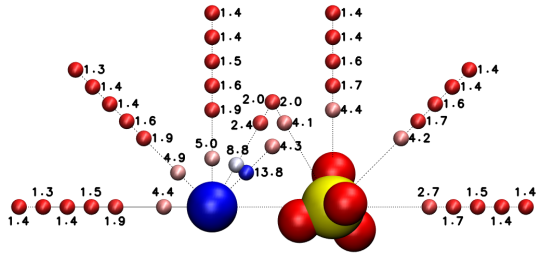

(c) $(\vec{p},\vec{p}_z)=(0.26,-0.14)$ $|e|$Å

Fig. 11 Average reorientation decay times (ps) of OH groups belonging to different water subpopulations around $MgSO_4$ SIP_i ion pairs with fixed ion configuration and orientation. The color scale of the smaller spheres conveys, for each panel, the magnitude of the reorientation time shown next to the spheres. Consecutive water subpopulations along the dashed lines are 1 or 2 Å apart. The subpopulations closest to Mg^{2+} are at $d=2$ Å and those closest to SO_4^{2-} at $d=4$ Å. The subpopulations at $(Mg^{2+},2Å,0^\circ)$ are only shown when they are sufficiently large to allow a good-quality fit to the $P_2(t)$ curve.

18 H. Yu, T. W. Whitfield, E. Harder, G. Lamoureux, I. Vorobyov, V. M. Anisimov, J. MacKerell, Alexander D. and B. Roux, *J. Chem. Theory Comput.*, 2010, **6**, 774–786.

19 H. T. Kim and W. J. Frederick, *J. Chem. Eng. Data*, 1988, **33**, 177–184.

20 *CRC handbook of chemistry and physics*, ed. W. M. Haynes, Taylor & Francis, 2011, ch. Concentrative properties of aqueous solutions: density, refractive index, freezing point depression, and viscosity, pp. 5–123–5–148.

21 M. J. Frisch, G. W. Trucks, H. B. Schlegel, G. E. Scuseria, M. A. Robb, J. R. Cheeseman, G. Scalmani, V. Barone, B. Mennucci, G. A. Petersson, H. Nakatsuji, M. Caricato, X. Li, H. P. Hratchian, A. F. Izmaylov, J. Bloino, G. Zheng, J. L. Sonnenberg, M. Hada, M. Ehara, K. Toyota, R. Fukuda, J. Hasegawa, M. Ishida, T. Nakajima, Y. Honda, O. Kitao, H. Nakai, T. Vreven, J. A. Montgomery, Jr., J. E. Peralta, F. Ogliaro, M. Bearpark, J. J. Heyd, E. Brothers, K. N. Kudin, V. N. Staroverov, R. Kobayashi, J. Normand, K. Raghavachari, A. Rendell, J. C. Burant, S. S. Iyengar, J. Tomasi, M. Cossi, N. Rega, J. M. Millam, M. Klene, J. E. Knox, J. B. Cross, V. Bakken, C. Adamo, J. Jaramillo, R. Gomperts, R. E. Stratmann, O. Yazyev, A. J. Austin, R. Cammi, C. Pomelli, J. W. Ochterski, R. L. Martin, K. Morokuma, V. G. Zakrzewski, G. A. Voth, P. Salvador, J. J. Dannenberg, S. Dapprich, A. D. Daniels, . V. Farkas, J. B. Foresman, J. V. Ortiz, J. Cioslowski and D. J. Fox, *Gaussian 09 Revision D.01*.

22 R. J. Heaton, P. A. Madden, S. J. Clark and S. Jahn, *J. Chem. Phys.*, 2006, **125**, 144104.

23 M. Masia, *J. Phys. Chem. A*, 2013, **117**, 3221–3226.

24 R. E. Hester, R. A. Plane and G. E. Walrafen, *J. Chem. Phys.*, 1963, **38**, 249–250.

25 F. P. Daly, D. R. Kester and C. W. Brown, *J. Phys. Chem.*, 1972, **76**, 3664–3668.

26 R. M. Izatt, D. Eatough, J. J. Christensen and C. H.

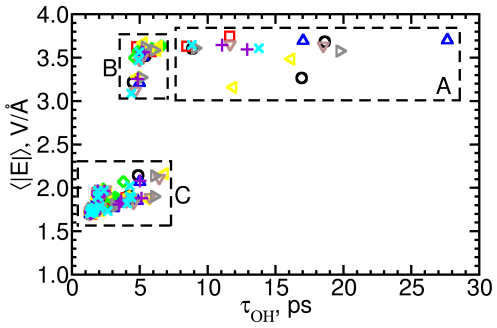

(a)

Fig. 12 Electric field magnitude, $\langle|\vec{E}|\rangle$, as a function of the reorientation time of water OH groups belonging to different water subpopulations around $MgSO_4$ SIP_i ion pairs with fixed ion orientation. For comparison, data for SIP_i, SIP_o and 2SIP with freely rotating ions is also included.

Bartholomew, *J. Chem. Soc. A*, 1969, 47–53.

27 J. W. Larson, *J. Phys. Chem.*, 1970, **74**, 3392–3396.

28 M. Eigen and U. K. Tamm, *Zeitschrift für Elektrochemie, Berichte der Bunsengesellschaft für physikalische Chemie*, 1962, **66**, 107–121.

29 A. R. Davis and B. G. Oliver, *J. Phys. Chem.*, 1973, **77**, 1315–1316.

30 G. Atkinson and S. Petrucci, *J. Phys. Chem.*, 1966, **70**, 3122–3128.

31 W. W. Rudolph, G. Irmer and G. T. Hefter, *PCCP*, 2003, **5**, 5253–5261.

32 R. Buchner, T. Chen and G. Hefter, *J. Phys. Chem. B*, 2004, **108**, 2365–2375.

33 T. Chen, G. Hefter and R. Buchner, *J. Phys. Chem. A*, 2003, **107**, 4025–4031.

34 E. Brandes, C. Stage, H. Motschmann, J. Rieder and R. Buchner, *J. Chem. Phys.*, 2014, **141**, 18C509.

35 J. J. Max and C. Chapados, *J. Chem. Phys.*, 2000, **113**, 6803–6814.

36 J. J. Max and C. Chapados, *J. Chem. Phys.*, 2001, **115**, 2664–2675.

37 A. A. Zavitsas, *Chem. Eur. J.*, 2010, **16**, 5942–5960.

38 J. Gujt, M. Bešter-Rogač and B. Hribar-Lee, *J. Mol. Liq.*, 2014, **190**, 34–41.

39 R. M. Fuoss, *Proc. Natl. Acad. Sci. USA*, 1980, **77**, 34–38.

40 J.-C. Justice and R. M. Fuoss, *J. Phys. Chem.*, 1963, **67**, 1707–1708.

41 S. H. Northrup and J. T. Hynes, *J. Chem. Phys.*, 1980, **73**, 2700–2714.

42 I. S. Joung and I. Cheatham, Thomas E., *J. Phys. Chem. B*, 2009, **113**, 13279–13290.

43 A. Vila Verde and R. Lipowsky, *J. Phys. Chem. B*, 2013, **117**, 10556–10566.

44 S. T. van der Post and H. J. Bakker, *PCCP*, 2012, **14**, 6280–6288.

45 S. T. van der Post, K.-J. Tielrooij, J. Hunger, E. H. G. Backus and H. J. Bakker, *Farad. Discuss.*, 2013, **160**, 171–189.

46 C. H. Giammanco, D. B. Wong and M. D. Fayer, *J. Phys. Chem. B*, 2012, **116**, 13781–13792.